JACS
JOURNAL OF THE AMERICAN CHEMICAL SOCIETY
Article
pubs.acs.org/JACS

Anomalous Compression of $D_5(450)$-C_{100} by Encapsulating La_2C_2 Cluster instead of La_2

Wenting Cai, Lipiao Bao, Shasha Zhao, Yunpeng Xie, Takeshi Akasaka, and Xing Lu*

State Key Laboratory of Materials Processing and Die & Mold Technology, School of Materials Science and Engineering, Huazhong University of Science and Technology (HUST), Wuhan 430074, China

Supporting Information

ABSTRACT: We demonstrate that a finite-length (10,0) carbon nanotube (CNT) with two fullerene caps, namely $D_5(450)$-C_{100}, is an ideal prototype to study the mechanical responses of small CNTs upon endohedral metal doping. Encapsulation of a large La_2C_2 cluster inside $D_5(450)$-C_{100} induces a 5% axial compression of the cage, as compared with the structure of $La_2@D_5(450)$-C_{100}. Detailed crystallographic analyses reveal quantitively the flexibility of the [10]cyclacene-sidewall segment and the rigidity of the pentagon-dominating caps for the first time. The internal C_2-unit acts as a molecular spring that attracts the surrounding cage carbon atoms through strong interactions with the two moving lanthanum ions. This is the first crystallographic observation of the axial compression of CNTs caused by the internal stress, which enhances our knowledge about the structural deformation of novel carbon allotropes at the atomic level.

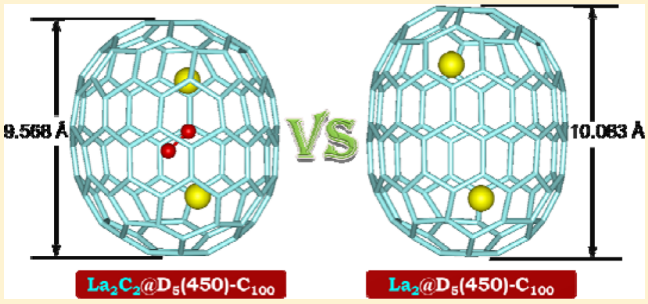

INTRODUCTION

Fullerenes are spherical carbon molecules that are soluble in common organic solvents. This feature advances fullerene isomers readily isolable with solution chromatography and structurally determinable with NMR spectroscopy and/or single crystal XRD crystallography.[1] In clear contrast, another well-known carbon allotrope, carbon nanotubes (CNTs), is totally insoluble in organic solvents and thus is difficult to characterize their structures accurately from an experimental viewpoint.[2] However, there is no clear boundary between fullerenes and CNTs.[3] For instance, although the prototypical I_h-C_{60} is ideally spherical, some higher fullerene cages exhibit elongated structures with a distinct long axis. To date, the nanotube-like fullerenes that have been crystallographically identified are $D_{5h}(1)$-C_{90}, $D_{3d}(3)$-C_{96}, $D_{5d}(1)$-C_{100}, and $D_2(812)$-C_{104}.[4−8] A notable feature of these nanotube-like structures is the existence of at least one layer of cyclo-paraphenylene (CPP) or cyclacene, which is the shortest sidewall segment of either an armchair CNT or a zigzag CNT, respectively.[9]

In this regard, the tubular appearance of higher fullerenes presents a clear connection with finite-length nanotubes capped with fullerene hemispheres at the two ends. There has long been believed that end-cap and finite-size effects should play an essential role in determining the geometrical and electronic properties of the capped nanotubes.[10−15] However, the corresponding research is merely limited to the theoretical realm because of the difficulties lying in the selective synthesis of "pure" CNTs with identical diameter/chirality[16,17] and the limitations of the characterization techniques at the angstrom scale. For instance, computational results from Yumura et al. demonstrated that the capped and uncapped finite-length CNTs adopt different bond-length alternation patterns, with the capped ones being more rigid.[18] Also, theoretical results from different groups proposed that the fullerene hemispheres strongly influence the vibrational modes and even the nucleation of finite-length CNTs.[19,20] Thus, the desire to investigate the behaviors of the side-wall segment of CNTs and the hemispherical caps against mechanical or electronic forces is fundamentally important.

Here we demonstrate that the flexibility of CNTs is preserved in nanotubular fullerenes under the internal stress by presenting single-crystal X-ray crystallographic results of a lanthanum-carbide-cluster-containing EMF, $La_2C_2@D_5(450)$-C_{100}, whose cage structure resembles the sidewall segment of a (10,0)-CNT. Surprisingly, we discover that encapsulation of a large metal cluster La_2C_2 compresses the long axis of $La_2C_2@D_5(450)$-C_{100} to a degree of up to 5%, as compared with the X-ray structure of $La_2@D_5(450)$-C_{100}. More meaningfully, we find that the deformation mainly occurs at the CPP sidewall fragment of $D_5(450)$-C_{100}, which has a response to the internal stress about three to six times higher than that of the pentagon-dominating caps. The C_2-unit acts as a molecular spring that contracts the cage via strong interactions with the two moving lanthanum ions.

Received: June 2, 2015
Published: July 28, 2015

ACS Publications © 2015 American Chemical Society

DOI: 10.1021/jacs.5b05668
J. Am. Chem. Soc. 2015, 137, 10292−10296

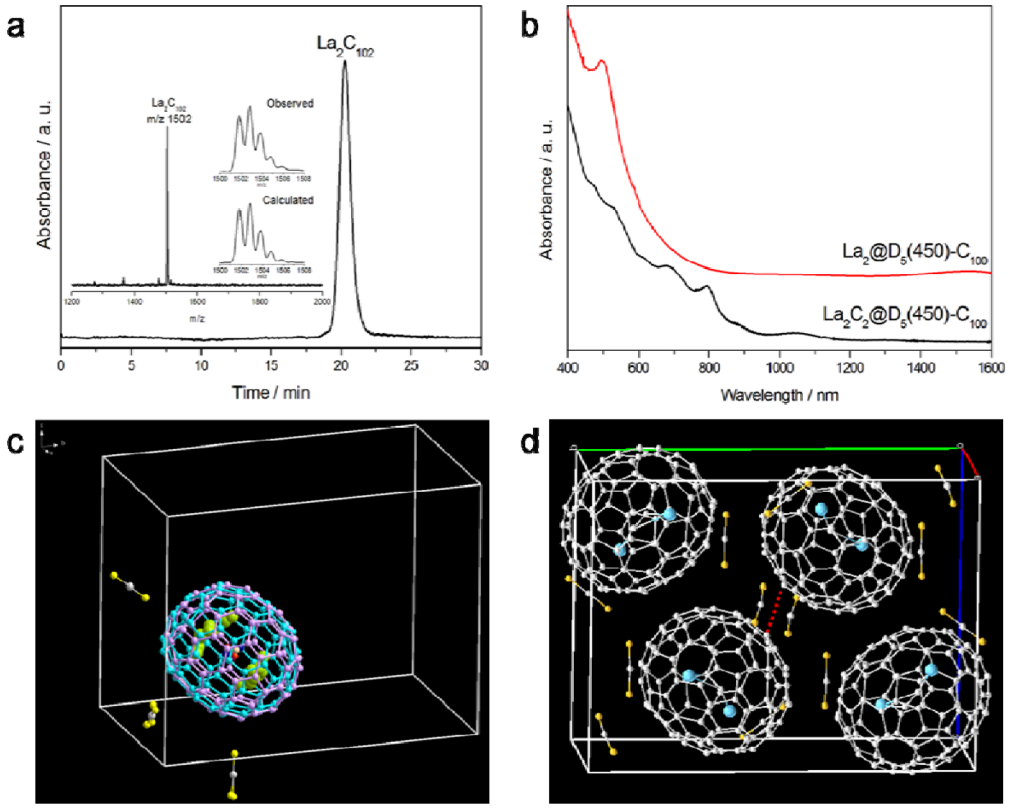

Figure 1. Characterization of $La_2C_2@D_5(450)$-C_{100}. (a) HPLC chromatogram of purified La_2C_{102} on a Buckyprep column with chlorobenzene as the eluent (HPLC conditions: flow rate, 0.7 mL min^{-1}; detection wavelength, 330 nm). The inset shows the LDI-TOF mass spectrum and expansions of the observed and calculated isotope distributions of La_2C_{102} in a negative ion mode. (b) Vis-NIR absorption spectrum of purified $La_2C_2@D_5(450)$-C_{100} dissolved in chlorobenzene in comparison with that of $La_2@D_5(450)$-C_{100}. (c) A view of $La_2C_2@D_5(450)$-C_{100}·$3(CS_2)$ in the asymmetric crystal unit. (d) Molecular packing of $La_2C_2@D_5(450)$-C_{100}·$3(CS_2)$ with minor disordered components omitted for clarity. The red dashed line emphasizes the closest C−C distance (3.344 Å) between two $La_2C_2@D_5(450)$-C_{100} molecules.

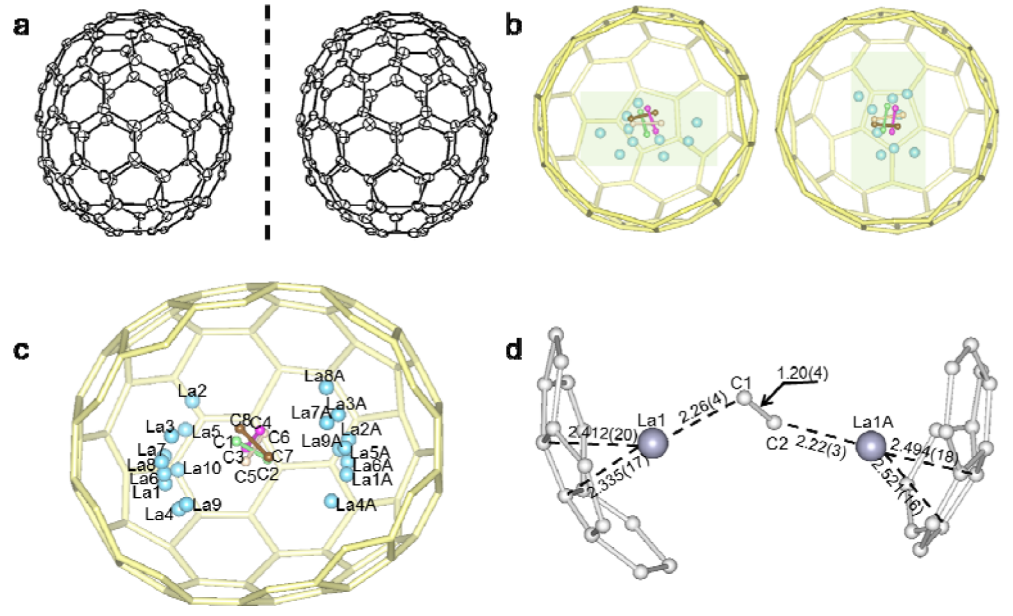

Figure 2. Single-crystal X-ray structure of $La_2C_2@D_5(450)$-C_{100}. (a) ORTEP drawings of the two enantiomers of $La_2C_2@D_5(450)$-C_{100} with thermal ellipsoids shown at the 5% probability level. Only the carbon cage is shown, and the disordered sites of the metallic cluster are omitted for clarity. (b) The distribution of La positions beneath the two poles of the cage as viewed down the five-fold axis of the major enantiomer of $D_5(450)$-C_{100}. (c) Drawing showing the positions of the disordered lanthanum sites relative to the C_2-unit in $La_2C_2@D_5(450)$-C_{100}. The lanthanum site occupancy: La1, 0.15; La2, 0.03; La3, 0.08; La4, 0.08; La5, 0.05; La6, 0.14; La7, 0.13; La8, 0.13; La9, 0.1; La10, 0.11; La1A, 0.20; La2A, 0.08; La3A, 0.14; La4A, 0.04; La5A, 0.14; La6A, 0.11; La7A, 0.05; La8A, 0.16; La9A, 0.08. (d) Relative position of the major La_2C_2 cluster with respect to the major enantiomer of $D_5(450)$-C_{100}.

DOI: 10.1021/jacs.5b05668
J. Am. Chem. Soc. 2015, 137, 10292−10296

RESULTS AND DISCUSSION

Characterization of $La_2C_2@D_5(450)$-C_{100}. La_2C_{102} was synthesized with a direct current arc discharge method and was isolated with multistage HPLC techniques (see Figures S1−S4, Supporting Information). Figure 1a shows the HPLC chromatogram and mass spectrum of purified La_2C_{102}. The molecular structure of La_2C_{102} is unambiguously determined with single crystal X-ray diffraction (XRD) crystallography. It is evident that this compound has a carbide structure, that is, $La_2C_2@C_{100}$. Analysis of cage connectivity reveals the cage isomer of $D_5(450)$-C_{100}, according to the spiro algorithm.[21] The vis-NIR spectrum exhibits distinct absorptions at 1045, 793, 689, 614, 513, and 471 nm, which differs from that of $La_2@D_5(450)$-C_{100},[22] indicative of their different electronic configurations (Figure 1b).

Usually a co-crystallization host such as Ni^{II}(OEP) (OEP = 2,3,7,8,12,13,17,18-octaethylporphin dianion) is used to make neat fullerene/endofullerene crystals suitable for XRD measurements. Even for the only example of solvated metallofullerene crystal, 1/4($Sc_3N@C_{80}$)·3/4(*p*-xylene), aromatic solvent molecules are necessary to provide $\pi-\pi$ and CH$-\pi$ interactions to halt the motion of the fullerene molecules.[23] Surprisingly, in our case of $La_2C_2@D_5(450)$-C_{100}, merely the fullerene and the intercalated CS_2 molecules exist (Figure 1c), although a benzene solution of Ni^{II}(OEP) and a CS_2 solution of the fullerene have been used for single crystal growth. This indicates that the tubular appearance of the cage facilitates the growth of single crystals. Figure 1d shows the packing structure of $La_2C_2@D_5(450)$-C_{100}·3(CS_2). The nearest cage−cage distance is 3.344 Å, featuring weak $\pi-\pi$ stacking interactions.

Single-Crystal X-ray Structure of $La_2C_2@D_5(450)$-C_{100}. The structure shows some degree of disorder in terms of both the fullerene cage and the internal La_2C_2 cluster. Chiral fullerene cage is disordered with two enantiomers possessing nearly equal occupancy (0.52:0.48). Figure 2a presents these two enantiomers, with the internal cluster omitted for clarity. Within the cage, there are 19 sites for the two La atoms. Figure 2b shows how these disordered La positions are arranged about the C_2 unit as viewed down the five-fold axis of the cage. Ten of them, which position under one terminal of the cage, are seemingly perpendicular to the rest nine sites beneath the canopy on the other side of the cage. Figure 2c shows a view of the La positions and the C_2 unit looking down the shortest cage axis. The La sites on the left side of the C_2 unit have occupancies ranging from 0.15 to 0.03, while the La positions on the right side of the C_2 unit are assigned occupancies that range from 0.20 to 0.04. The C_2 unit exhibits four disordered positions in total with C−C distances falling in the range of 1.00−1.21 Å (see Table S1, Supporting Information). They have similar occupancy values of 0.30, 0.29, 0.21, and 0.20, respectively. The large number of La sites and C_2 units indicates the free movement of metal atoms and the flexible swing of the C_2 unit about the inner space of the carbon cage. Despite the considerable disorder in the La positions and the C_2 unit, the major sites of the La atoms are slightly displaced from the five-fold axis of the carbon cage. Figure 2d presents some details regarding the location of the major La_2C_2 site in $La_2C_2@D_5(450)$-C_{100}. Each La ion situates over a respective [6,6]-bond junction near a pole of the cage that the five-fold axis of the cage passes. The La···La separation for the most populated sites is 4.83 Å, while the shortest La···C distances for the most populated sites fall in the range of 2.22−2.52 Å. The dihedral angle between the two LaC_2 portions is about 141.3°, indicating a bent configuration of La_2C_2 cluster. More meaningfully, the C_2 unit is found to rotate in the cluster plane, thus confirming the computational prediction from Dorn and co-workers that the linear M_2C_2 cluster structures are feasible if the fullerene cage is a relatively large cage of at least 100 carbons.[24] However, theoretical results from Popov et al. proposed that the distorted linear structure of M_2C_2, relative to the common butterfly-like configurations, can also be attributed to the long metal−metal distance, which induces a "nanoscale stretching" effect on the cluster.[25]

Although previous reports demonstrated that M_2C_2 (M = Sc, Y, Er, Ti, Gd) can be readily entrapped inside fullerenes,[26] this is the first crystallographic confirmation that a relatively large La_2C_2 cluster is successfully encapsulated inside a fullerene cage. For the carbide species, smaller rare-earth atoms such as Sc and Y can form M_2C_2-containing EMFs having cage sizes between C_{80} and C_{84}, whereas the larger Gd_2C_2 cluster templates a C_{92} cage, and the largest La_2C_2 in our finding prefers larger cages of at least 100 carbons. In other words, for endohedrals of the $M_2C_2@C_{2n}$-type, as the size of the metal ions increase, gradual increase in the abundance of the larger cages is observed. This result could be a useful tip for the high yield synthesis of large fullerenes.

The Anomalous Axial Compression of $D_5(450)$-C_{100}. Recently, a dimetallofullerene utilizing the $D_5(450)$-C_{100} carbon cage encapsulating two lanthanum ions, $La_2@D_5(450)$-C_{100}, was isolated and structurally identified with single-crystal XRD crystallography by Balch and co-workers.[22] The length of the cage, as measured by the centroid-to-centroid distance between the two pentagons on the five-fold axis, is 10.083 Å, and the width of the cage, which is determined by the average distance of the C_2 axes, is 8.024 Å.[22] In contrast, our single crystal X-ray results demonstrate that the long axis of $La_2C_2@D_5(450)$-C_{100} shrinks into 9.585 Å, but the width of the cage slightly expands to 8.332 Å (Figure 3). This unambiguously confirms that the larger cluster La_2C_2 contracts the fullerene cage, instead of expanding it. In an effort to explain this abnormal phenomenon, the interactions between La ions and the carbon atoms are taken into account. As Table 1 shows, the La···La separation between the two predominant La atoms in $La_2@D_5(450)$-C_{100}

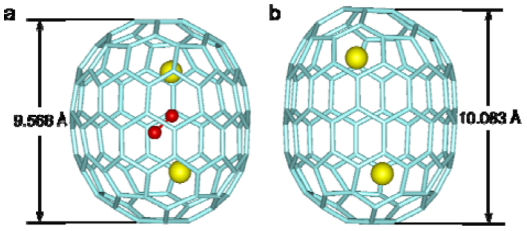

Figure 3. A comparison of X-ray structures of $D_5(450)$-C_{100} encapsulating different clusters. (a) $La_2C_2@D_5(450)$-C_{100} and (b) $La_2@D_5(450)$-C_{100}.[22]

Table 1. Cage Size, La···La Separations, and the Shortest La···Cage Distances of $La_2C_2@D_5(450)$-C_{100} and $La_2@D_5(450)$-C_{100}[22]

compound	length (Å)	width (Å)	La···La (Å)	La···cage (Å)
$La_2C_2@D_5(450)$-C_{100}	9.568	8.332	4.830	2.441
$La_2@D_5(450)$-C_{100}	10.083	8.024	5.744	2.445

DOI: 10.1021/jacs.5b05668
J. Am. Chem. Soc. 2015, 137, 10292−10296

(5.744 Å) is significantly larger than that in La_2C_2@D_5(450)-C_{100} (4.830 Å), while the La···cage distances are almost constant for both compounds. Obviously, the existence of the C_2 unit can partially neutralize the positive charge and reduce the Coulombic repulsions between the two La ions so as to shorten the La···La distance. Theoretical results proposed that both covalent and ionic interactions coexist between metal ions and carbon atoms in carbide cluster EMFs.[27] In view of this, the axial compression of the carbon cage might be attributed to the stronger bonding interactions between the La ions and the C_2 unit which acts as a molecular spring to contract the surrounding cage carbon atoms via interactions with the two La ions. Meanwhile, the moving La ions are supposed to be a "contributing factor" that induces the compression of carbon cage via enhanced interactions with the C_2 unit and the surrounding cage carbon atoms.

Crystallographic Observation of the Structural Deformation of a Capped Finite-Length CNT D_5(450)-C_{100}. It is worth noting that the axial compression has never been observed in spherical fullerene molecules, but it is a common behavior of carbon nanotubes. For example, theoretical results indicate that the critical failure strain of an (8,0) CNT under axial compressive loadings is about 12%,[28] while even larger critical axial strain (about 45%) is achieved with theory for SWNTs filled with high-density molecules.[29] However, the related experimental results are extremely rare. Here we show for the first time with X-ray crystallographic results that the flexibility of carbon nanotubes is preserved in the nanotubular fullerenes. More meaningfully, we show below that the tubular cage can also be compressed along the axis upon internal stress and that the existence of pentagons in the framework plays a critical role in differentiating the deformation behaviors of the sidewalls and spherical caps of capped finite-length CNTs (vide infra).

The axial strain is defined as the length change of the carbon nanotube divided by the initial length.[30] Thus, the whole axial strain of this small capped zigzag (10,0) nanotube, D_5(450)-C_{100}, is calculated to be 5% from the X-ray results of La_2C_2@D_5(450)-C_{100} and La_2@D_5(450)-C_{100}. In order to clearly delineate the different effect of compression on the caps and the cylindrical sidewall segment, the D_5(450)-C_{100} cage is divided into six layers (Figure 4). Whereas layers 3 and 4 correspond to the CPP sidewall of the D_5(450)-C_{100} containing ten [6,6]-bonds along the 5-fold axis of the cage, layers 1 and 6 stand for the end-caps composed of five [6,6]-bonds along the 5-fold axis. Notably, layers 2 and 5 contain merely 10 [5,6]-bonds along the 5-fold axis of the cage, without any [6,6]-bond. The total axial strain of each layer is calculated according to the average C−C bond lengths of D_5(450)-C_{100} from the single-crystal X-ray results of La_2C_2@D_5(450)-C_{100} and La_2@D_5(450)-C_{100} (see Table S2, Supporting Information). As shown in Figure 4, the compression occurs in the end-caps (layers 2 and 5) of this finite-length capped zigzag (10,0) nanotube is about 0.2−0.4%, while that in the side-wall segment (layers 3 and 4) is more than 1.2%. The difference is obviously caused by the existence of pentagons in the framework because the deformation degree of the [6,6]-bonds along the tube axis, especially those on the side-wall segments (layers 3 and 4), is higher than the corresponding [5,6]-bonds. Our crystallographic results quantitively confirm that the existence of pentagons in CNT-sidewalls could fundamentally enhance the rigidity to an extent of three to six times. Along this line, with the insertion of pentagons, one can tune the mechanical properties of carbon nanotubes effectively.

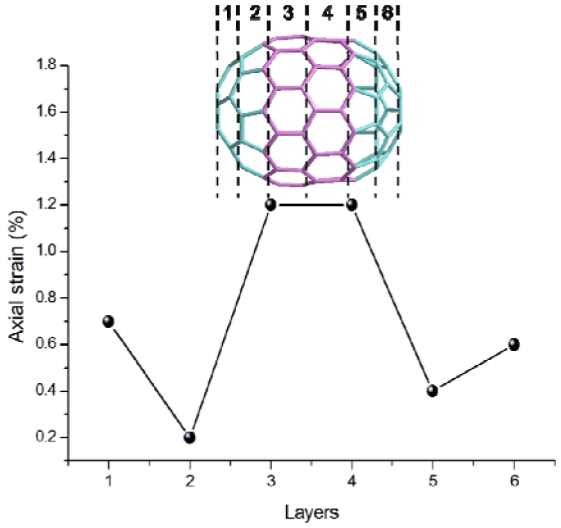

Figure 4. Axial strains of different regions in the small capped zigzag (10,0) nanotube D_5(450)-C_{100}. Layers 3 and 4 represent the [10]cyclacenes, while others stand for the two fullerene caps. The values are calculated from the X-ray results of La_2C_2@D_5(450)-C_{100} and La_2@D_5(450)-C_{100}.[22]

CONCLUSIONS

In this work, the X-ray structure of a La_2C_2-containing EMF, La_2C_2@D_5(450)-C_{100}, reveals that the flexibility of carbon nanotubes is preserved in nanotubular fullerenes under internal stress. Amazingly, we find that the encapsulation of a large La_2C_2 cluster induces an axial compression of the D_5(450)-C_{100} cage to a degree of about 5%. Detailed analyses reveal that the structural deformation mainly occurs in the [10]cyclacenes sidewall segment, which contains purely [6,6]-bonds, whereas the pentagon-dominating corannulene caps are very rigid. We present the first single-crystal X-ray crystallographic evidence for the mechanical deformation of finite-length capped CNTs, and the results are useful in future works of rational design and mechanical applications of CNTs. For instance, by introducing pentagon into the CNT frameworks, one may selectively alter the rigidity of the tubes.

EXPERIMENTAL SECTION

Synthesis and Isolation of La_2C_{102}. Soot-containing lanthanum metallofullerenes were synthesized using the direct current arc discharge method. The raw soot was refluxed in 1,2,4-trichlorobenzene (TCB) under a nitrogen atmosphere for 15 h. After removal of TCB, the residue was dissolved in toluene and was subjected to a four-stage high-performance liquid chromatography (HPLC) separation process. Further details are described in Supporting Information.

Spectroscopic Measurements. Laser desorption ionization time-of-flight (LDI-TOF) mass spectrometry was measured on a BIFLEX III spectrometer (Bruker Daltonics Inc., Germany). Vis-NIR spectrum was measured on a PE Lambda 750S UV−vis-NIR spectrophotometer (PerkinElmer, America) in chlorobenzene.

Single-Crystal X-ray Diffraction. Crystalline blocks of La_2C_{102} were obtained by layering a benzene solution of Ni^{II}(OEP) over a nearly saturated solution of the endohedral in CS_2 in a glass tube. Over a 20-day period, the two solutions diffused together, and black crystals formed. A piece of crystal with dimensions of 0.16 × 0.13 × 0.09 mm was chosen for the single-crystal XRD measurement and provided all the structural information about La_2C_2@D_5(450)-C_{100}. XRD measure-

DOI: 10.1021/jacs.5b05668
J. Am. Chem. Soc. 2015, 137, 10292−10296

ment was performed at 173 K on a Bruker D8 QUEST machine equipped with a CMOS camera (Bruker AXS Inc., Germany). The multiscan method was used for absorption corrections. The structure was solved by direct method and was refined with SHELXL-2013.[31] Crystal data for $La_2C_2@D_5(450)$-C_{100}·3(CS_2): $C_{105}La_2S_6$, M_w = 1731.23, monoclinic, space group $P2_1/n$, a = 12.3310(19) Å, b = 23.721(4) Å, c = 18.341(3) Å, β= 94.460(2)°, V = 5348.5(14) Å^3, Z = 4, T = 173(2) K, ρ_{calcd} = 2.150 Mg m^{-3}, μ(Mo Kα) = 1.885 mm^{-1}, 61,304 reflections measured, 14,905 unique (R_{int} = 0.0421) used in all calculations. The final wR_2 was 0.4384 (all data) and R_1 (8220 with $I > 2\s(I)$) = 0.1246. The relatively high R_1 and wR_2 values are due to the severe disorder in the cage, the metal cluster, and the intercalated solvent molecules. CCDC 1037067 contains the crystallographic data.

■ ASSOCIATED CONTENT

Supporting Information

The Supporting Information is available free of charge on the ACS Publications website at DOI: 10.1021/jacs.5b05668.

Characterization data (CIF)

HPLC profiles for the separation of $La_2C_2@D_5(450)$-C_{100}; correlation between $D_5(450)$-C_{100} and (10,0) zigzag end-capped carbon nanotube; selected X-ray results of $La_2C_2@D_5(450)$-C_{100} and $La_2@D_5(450)$-C_{100} (PDF)

■ AUTHOR INFORMATION

Corresponding Author

*lux@hust.edu.cn

Notes

The authors declare no competing financial interest.

■ ACKNOWLEDGMENTS

X.L. thanks Sumio Iijima for valuable discussions. X.L. and T.A. are grateful to the students and infrastructures in University of Tsukuba for producing part of the raw materials containing La_2C_{102}. Financial support from The National Thousand Talents Program of China, NSFC (21171061, 51472095). Program for Changjiang Scholars and Innovative Research Team in University (IRT1014) to X.L. is faithfully acknowledged.

■ REFERENCES

(1) Kratschmer, W.; Lamb, L. D.; Fostiropoulos, K.; Huffman, D. R. *Nature* **1990**, *347*, 354−358.

(2) Iijima, S. *Nature* **1991**, *354*, 56−58.

(3) Smalley, R. E.; Haufler, R. E. Electric arc process for making fullerenes. U.S. Patent 5,227,038, July 13, 1993.

(4) Curl, R. F. *Angew. Chem., Int. Ed. Engl.* **1997**, *36*, 1566−1576.

(5) Yang, H.; Beavers, C. M.; Wang, Z. M.; Jiang, A.; Liu, Z. Y.; Jin, H. X.; Mercado, B. Q.; Olmstead, M. M.; Balch, A. L. *Angew. Chem., Int. Ed.* **2010**, *49*, 886−890.

(6) Yang, H.; Jin, H. X.; Che, Y. L.; Hong, B.; Liu, Z. Y.; Gharamaleki, J. A.; Olmstead, M. M.; Balch, A. L. *Chem. - Eur. J.* **2012**, *18*, 2792−2796.

(7) Fritz, M. A.; Kemnitz, E.; Troyanov, S. I. *Chem. Commun.* **2014**, *50*, 14577−14580.

(8) Yang, S. F.; Wei, T.; Kemnitz, E.; Troyanov, S. I. *Chem. - Asian J.* **2014**, *9*, 79−82.

(9) Omachi, H.; Nakayama, T.; Takahashi, E.; Segawa, Y.; Itami, K. *Nat. Chem.* **2013**, *5*, 572−576.

(10) Yumura, T.; Hirahara, K.; Bandow, S.; Yoshizawa, K.; Iijima, S. *Chem. Phys. Lett.* **2004**, *386*, 38−43.

(11) Chen, C.; Tsai, C.-C.; Lu, J.-M.; Hwang, C.-C. *J. Phys. Chem. B* **2006**, *110*, 12384−12387.

(12) Miyauchi, Y.; Chiashi, S.; Murakami, Y.; Hayashida, Y.; Maruyama, S. *Chem. Phys. Lett.* **2004**, *387*, 198−203.

(13) Harigaya, K. *Phys. Rev. B: Condens. Matter Mater. Phys.* **1992**, *45*, 12071−12076.

(14) Sato, T.; Tanaka, M.; Yamabe, T. *Synth. Met.* **1999**, *103*, 2525−2526.

(15) Cioslowski, J.; Rao, N.; Moncrieff, D. *J. Am. Chem. Soc.* **2002**, *124*, 8485−8489.

(16) Yang, F.; Wang, X.; Zhang, D. Q.; Yang, J.; Luo, D.; Xu, Z. W.; Wei, J. K.; Wang, J. Q.; Xu, Z.; Peng, F.; Li, X. M.; Li, R. M.; Li, Y. L.; Li, M. H.; Bai, X. D.; Ding, F.; Li, Y. *Nature* **2014**, *510*, 522−524.

(17) Sanchez-Valencia, J. R.; Dienel, T.; Groning, O.; Shorubalko, I.; Mueller, A.; Jansen, M.; Amsharov, K.; Ruffieux, P.; Fasel, R. *Nature* **2014**, *512*, 61−64.

(18) Yumura, T.; Bandow, S.; Yoshizawa, K.; Iijima, S. *J. Phys. Chem. B* **2004**, *108*, 11426−11434.

(19) Lair, S.; Herndon, W.; Murr, L.; Quinones, S. *Carbon* **2006**, *44*, 447−455.

(20) Yumura, T.; Nozaki, D.; Bandow, S.; Yoshizawa, K.; Iijima, S. *J. Am. Chem. Soc.* **2005**, *127*, 11769−11776.

(21) Fowler, P. W.; Manolopoulos, D. E. *An Atlas of Fullerenes*; Dover Publications, Inc.: Mineola, NY, 2006.

(22) Beavers, C. M.; Jin, H.; Yang, H.; Wang, Z. M.; Wang, X.; Ge, H.; Liu, Z.; Mercado, B. Q.; Olmstead, M. H.; Balch, A. L. *J. Am. Chem. Soc.* **2011**, *133*, 15338−15341.

(23) Hernandez-Eguia, L. P.; Escudero-Adan, E. C.; Pinzon, J. R.; Echegoyen, L.; Ballester, P. *J. Org. Chem.* **2011**, *76*, 3258−3265.

(24) Zhang, J. Y.; Fuhrer, T.; Fu, W. J.; Ge, J. C.; Bearden, D. W.; Dallas, J.; Duchamp, J.; Walker, K.; Champion, H.; Azurmendi, H.; Harich, K.; Dorn, H. C. *J. Am. Chem. Soc.* **2012**, *134*, 8487−8493.

(25) Deng, Q.; Popov, A. A. *J. Am. Chem. Soc.* **2014**, *136*, 4257−4264.

(26) Lu, X.; Akasaka, T.; Nagase, S. *Acc. Chem. Res.* **2013**, *46*, 1627−1635.

(27) Guo, Y. J.; Yang, T.; Nagase, S.; Zhao, X. *Inorg. Chem.* **2014**, *53*, 2012−2021.

(28) Srivastava, D.; Menon, M.; Cho, K. *Phys. Rev. Lett.* **1999**, *83*, 2973−2976.

(29) Ni, B.; Sinnott, S. B.; Mikulski, P. T.; Harrison, J. A. *Phys. Rev. Lett.* **2002**, *88*, 205505.

(30) Sears, A.; Batra, R. C. *Phys. Rev. B: Condens. Matter Mater. Phys.* **2006**, *73*, 085410.

(31) Sheldrick, G. M. *Acta Crystallogr., Sect. A: Found. Crystallogr.* **2008**, *64*, 112−122.

DOI: 10.1021/jacs.5b05668
J. Am. Chem. Soc. 2015, 137, 10292−10296